Electronic supplementary information

Origin of Metastable Oligomers and their Effects on Amyloid Fibril Self-Assembly

Filip Hasecke,‡[a] Tatiana Miti,‡[b] Carlos Perez,[b] Jeremy Barton,[b] Daniel Schölzel,[ac] Lothar Gremer,[ac] Clara S.R. Grüning,[a] Garrett Matthews,[b] Georg Meisl,[d] Tuomas P.J. Knowles,[d] Dieter Willbold,[ac] Philipp Neudecker,[ac] Henrike Heise,[ac] Ghanim Ullah,[b] Wolfgang Hoyer*[ac] and Martin Muschol*[b]

[a] *Institut für Physikalische Biologie, Heinrich-Heine-Universität, 40204 Düsseldorf, Germany. E-mail: wolfgang.hoyer@hhu.de*
[b] *Department of Physics, University of South Florida, Tampa, FL 33620, USA. E-mail: mmuschol@usf.edu*
[c] *Institute of Complex Systems (ICS-6), Structural Biochemistry, Research Centre Jülich, Germany.*
[d] *Department of Chemistry, University of Cambridge, Lensfield Road, Cambridge CB2 1EW, UK.*

Contents

Materials and methods

Protein and chemicals

Two times recrystallized, dialyzed, and lyophilized hewL was purchased from Worthington Biochemicals (Lakewood, NJ) and used for all experiments. Ultrapure grade ThT was obtained from Anaspec (Freemont, CA) and standard grade ThT from Sigma Aldrich. All other chemicals were from Fisher Scientific (Pittsburgh, PA) and were reagent grade or better.

Preparation of hewL solutions

HewL was dissolved at twice its final concentration in 25 mM KH_2PO_4 pH 2 buffer and was placed in a water bath for 3 minutes at 42 °C to help dissolve preformed assemblies. Samples were successively filtered through 220 nm nitrile (Fisherbrand, Fisher Scientific, Pittsburgh, PA) and 50 nm polyethersulfone (Tisch Scientific, North Bend, OH) pore size syringe filters. The concentrated hewL stock was mixed 1:1 with a NaCl/25 mM KH_2PO_4 pH 2 stock solution at double the desired final salt concentrations. Final lysozyme concentrations were determined from UV absorption measurements at 280 nm (ε_{280} = 2.64 mL mg^{-1} cm^{-1}).

Preparation of DimAβ

Following a strategy previously established for recombinant production of Aβ,[1] bacterial expression of dimAβ was achieved by co-expression of ZAβ3, a binding protein that shields aggregation-prone sequence segments of Aβ. The gene encoding dimAβ, including an N-terminal methionine, followed by a Aβ40 unit, a $(G_4S)_4$ linker, and a second Aβ40 unit, was obtained from Life Technologies, and was cloned into the pACYCDuet-1 vector for co-expression with the ZAβ3 gene using NcoI and HindIII restriction sites. The coexpression vector contains the genes for dimAβ and $(His)_6$-tagged ZAβ3 in the following order: T7promoter-1 – dimAβ – T7promoter-2 – $(His)_6$ZAβ3 – T7 terminator. The protein was expressed as described.[1]

For purification, cell pellets were resuspended in 50 mM Na-phosphate, 0.3 M NaCl, 20 mM imidazole, pH 8, containing EDTA-free protease inhibitor (Roche Applied Sciences) and lysed by a cell disrupter (Constant Systems). The cell debris was removed by centrifugation in a Beckman J2-21 centrifuge mounting a JA20.1 rotor at 18,000 RPM, 4 °C for 40 minutes. For capture of the dimAβ:ZAβ3 complex by immobilized metal ion affinity chromatography (IMAC), the supernatant was loaded on a HisTrap FF column (GE Healthcare). DimAβ was separated from the resin-bound ZAβ3 and eluted with 8 M urea, 20 mM Na-phosphate, pH 7. For further purification, including removal of residual ZAβ3, reverse phase high-performance liquid chromatography (RP-HPLC) was performed. For this purpose the IMAC eluate was concentrated in a Vivaspin 20 centrifugal concentrator (Sartorius), followed by addition of 5 mM TCEP to reduce the disulfide bond of ZAβ3, and loading onto a semi-preparative Zorbax 300SB-C8 RP-HPLC column (9.4 mm × 250 mm, Agilent) connected to an Agilent 1260 Infinity system with UV detection at 214 nm. Monomeric dimAβ was eluted in a gradient from 30% (v/v) to 36% acetonitrile in water, 0.1% (v/v) trifluoroacetic acid at 80 °C. DimAβ containing fractions were pooled, lyophilized, dissolved in HFIP, aliquoted in 1 mg portions, lyophilized again, and stored at -20 °C. Immediately before use in experiments, lyophilized dimAβ was reconstituted in 6 M guanidinium-HCl, 50 mM Na-phosphate, 50 mM NaCl, pH 7.4, and sonicated for 30 minutes in a sonicator bath. Subsequently, the solution was loaded onto a Superdex 75 10/300 GL column (GE Healthcare) equilibrated with 35 mM Na_2HPO_4, 50 mM NaCl, 5 mM NaOH, pH 11.

DimAβ eluted at 13.5 ml. Protein concentration was determined by spectrophotometry. Immediately before the start of an experiment, 1.5% 1 M NaH_2PO_4 was added, yielding 50 mM Na-phosphate, 50 mM NaCl, pH 7.4, as final buffer.

Atomic force microscopy

For imaging of hewL assemblies, 50 µL of sample solutions were diluted 20-100 fold into the same solvent used during growth, deposited onto freshly cleaved mica for 3 minutes, rinsed with deionized water and dried with dry nitrogen. Amyloid fibrils were imaged in air with a MFP-3D atomic-force microscope (Asylum Research, Santa Barbara, CA) using NSC36/NoAl (Mikromasch, San Jose, CA) or PFP-FMR-50 (Nanosensor, Neuchatel, Switzerland) silicon tips with nominal tip radii of 10 and 7 nm, respectively. The cantilever had a typical spring constant and resonance frequency of 2 nN/nm and 80 kHz, respectively. It was driven at 60−70 kHz in alternating current mode and at a scan rate of 0.25-0.75 Hz. Images were acquired at 512 × 512 pixel resolution. Raw image data were corrected for image bow and slope. Amplitude, phase, and height images were collected for areas of 5x5 µm.

For imaging of dimAβ assemblies, 25 µL of sample solutions were directly deposited onto freshly cleaved mica for 1 minute, rinsed with deionized water and dried with dry nitrogen. Imaging was performed in air with a NanoWizard 2 (JPK instruments) with OMCLAC160TS silicon cantilevers (Olympus) with a nominal tip radius of 7 nm. The cantilever had a typical spring constant and resonance frequency of 26 nN/nm and 300 (±100) kHz, respectively. It was driven at 250−370 kHz in intermittent contact mode and at scan rates of 0.5-1.0 Hz. Images were acquired at 1024 × 1024 pixel resolution. Raw image data were corrected for image bow and slope. Amplitude, phase, and height images were collected for areas of 2x2 or 10x10 µm. Height images were superimposed over either amplitude or phase images using Gimp – GNU Image Manipulation Program.

Circular dichroism spectroscopy

Far-UV CD spectra of dimAβ were measured on a JASCO J-815 spectropolarimeter at a protein concentration of 20 µM in 1 mm Suprasil Quarz cuvettes (Hellma). To obtain a spectrum of monomeric dimAβ the sample was measured at 4°C, immediately after elution of the monomer fraction from SEC. The spectrum of dimAβ in the gO/CF state was recorded at 20°C, after 24 hours of quiescent incubation in 50 mM Na-phosphate, 50 mM NaCl, pH 7.4. The gO/CF state of the sample was confirmed by AFM.

Thioflavin T (ThT) fluorescence-monitored amyloid formation

ThT stock solutions were prepared by dissolving 1 mM dye in distilled water and then filtering through 220 nm syringe filters. Final ThT concentrations were obtained from absorption at λ = 412 nm (ε_{412} = 32 000 M^{-1} cm^{-1}).

HewL amyloid growth kinetics measurements with ThT were performed using a SpectraMax M5 fluorescence plate reader (Molecular Devices). ThT fluorescence was excited at 440 nm, and emission collected at 488 nm. Protein solutions at concentrations ranging from 0.3 mg/ml (21 µM, below the COC) to 5 mg/ml (350 µM, above the COC) were incubated in the presence of either 450 or 500 mM NaCl. Protein concentrations were more closely spaced near the COC for a given salt concentration, and more widely spaced above the COC. Typically, six identical 300 µL samples were incubated in a 96 well plate at 52 °C.

ThT at final concentrations of 5-10 μM was added to each well. Measurements were taken every 20 minutes and the plate was shaken for 3 seconds before each measurement.

DimAβ amyloid growth kinetics measurements were performed using an Infinite M200 Pro fluorescence plate reader (Tecan) with ThT excitation at 445 nm, and emission collected at 482 nm. Protein concentrations ranged from 0.6 μM (below the COC) to 40 μM (above the COC) in 50 mM Na-phosphate, 50 mM NaCl, pH 7.4. Typically, three identical 100 μL samples were incubated in a 96 well plate at 37 °C. ThT at final concentrations of 100 μM was added to each well. Measurements were taken every 3 minutes and the plate was shaken for 2 seconds before each measurement. The slow thermal equilibration of the multiwell plates causes an initial decrease in ThT fluorescence, which is equally present in ThT/buffer control wells. This thermal transient was either removed from the traces (lysozyme) or ignored for the analysis of the more rapidly assembling dimAβ samples.

Determination of the COC

We frequently refer to the COC, which is the phase boundary for the onset of gO/CF formation in both hewL and dimAβ. For hewL, we relied on our prior measurements of a sharp transition in ThT and light scattering kinetics from traces with extended lag periods to the onset of a lag-free drift.[2] This transition coincided with a sudden switch in aggregate morphology from RFs past the lag period to immediate presence of gOs and CFs. In addition, we showed that pre-formed gO/CFs grew above and decayed below the COC and that RFs seeded above the COC continued to grow. These measurements indicated that the COC is a (metastable) phase boundary, and the resulting phase diagram is shown in Fig. 1B. For dimAβ, the COC was similarly taken as the concentration for which ThT kinetics transitioned from pure sigmoidal to weakly bimodal kinetics - again reflecting the lack of a lag period for gO/CF formation.

Data analysis of ThT kinetics

The sigmoidal kinetics of RF formation in the absence of oligomers (below the COC) was fit to the analytical approximation of nucleated polymerization with secondary nucleation mechanisms.[3] Specifically, in the absence of fibril seeding

$$M_{RF}(t) = M_0[1 - \exp\left(C_- e^{-\kappa t} - C_+ e^{+\kappa t} + \frac{\delta^2}{\kappa^2}\right)] \quad (1)$$

where M_{RF} is the fibril mass, M_0 the total protein concentration, $C_\pm = \pm(\delta/2\kappa)^2$, and δ and κ represent the primary and secondary nucleation rates.

The biphasic kinetics of dimAβ and hewL, in turn, were fit to a superposition of a one-step oligomerization reaction and the above nucleated-polymerization reaction. For dimAβ, the time regimes of dominant gO/CF formation and dominant RF formation were sufficiently separated to allow separate analysis of the gO/CF assembly kinetics. Two alternative reaction models were fit to gO/CF kinetics in the initial time regime, namely primary nucleation-growth and one-step oligomerization. For a match to primary nucleation-growth the expression for classical nucleated polymerization was used[4]

$$M_{gO/CF}(t) = M_0[1 - \mathrm{sech}^{2/n_c}\left(\sqrt{n_c k_n k_+ {M_0}^{n_c}}\, t\right)] \quad (2)$$

with $M_{gO/CF}$(t) the mass concentration of polymer, M_0 the total protein concentration, k_n the nucleation rate constant, k_+ the elongation rate constant, and n_c the critical nucleus size. Global fits to the concentration-dependent gO/CF formation were performed with n_c and the product $k_n k_+$ as shared fit parameters. For one-step oligomerization $n\,\mathrm{M} \rightarrow \mathrm{M}_n$, the mass concentration of oligomer, $M_{gO/CF}$, evolves in time according to the following expression

$$M_{gO/CF}(t) = M_0 - [M_0^{1-n} + (n-1)nkt\,]^{1/(1-n)} \quad (3)$$

with M_0 the total protein concentration, k the oligomerization rate constant, and n the oligomer size or reaction order. Global fits to the concentration-dependent gO/CF formation data were performed with n and k as shared fit parameters. For both fits, the proportionality constant relating M(t) to ThT fluorescence intensity was treated as a fit parameter with an individual value for every sample.

In the case of hewL, the time scales for gO/CF and RF formation overlapped, particularly at monomer concentrations just slightly above the COC. We therefore fit the data to the superposition of the above nucleated polymerization reaction (eqn. 1) and an oligomerization reaction. In addition, the initial hewL oligomerization kinetics were better approximated using a 1st-order forward reaction with an exponential growth in time.

$$M_{gO,CF}(t) = M_\infty(1 - \exp(-at)) \quad (4)$$

where $M_{gO/CF}$(t) is the mass concentration of oligomer, and M_∞ is the gO/CF mass that would be reached in the absence of RF formation. The neglect of a backward rate for oligomers is justified by two observations. First of all, we had previously shown that gO/CF decay rates are exceedingly small.[2] In addition, as discussed below, CFs did not fully depolymerize for many days after RFs had nucleated.

Determination of lag periods

We defined the RF lag time as the point at which the amplitude of the RF portion of the ThT signal increases beyond a fixed threshold. To determine RF lag periods below the COC (sigmoidal growth) ThT kinetics were directly fit to Eqn. (1). Above the COC (biphasic growth) our kinetics data were fit as the superposition of oligomeric and RF growth, as described above. The oligomeric fits were then subtracted from the entire time traces, resulting in the RF portion of the ThT signal. RF lag periods where then determined as below the COC. In both cases, using semi-logarithmically scaled ThT intensities significantly improves visual detection for deviations of ThT kinetics from its flat baseline and onset of significant RF growth. Error bars for individual lag periods (see Figs. 5E &F), which are derived from analytical fits to individual kinetic traces, are difficult to assign. However, the scatter among the data points is a reasonable measure of underlying experimental and fitting uncertainties. The uncertainty in the slope of the resulting power law fit through the lag periods, as well as the average of the slopes for three independent repeats of these experiments, is provided in the figure caption.

Stability assessment of dimAβ assembly states by ZAβ3

The affibody protein ZAβ3 and its tryptophan-containing derivative ZAβ3W were prepared as described previously.[5,6] To monitor the stability of dimAβ assemblies formed during ThT assays, 14 μM ZAβ3

was added to assembly reactions of 6 µM dimAβ at different time points, and ThT fluorescence was recorded. To test if RFs of dimAβ are thermodynamically or only kinetically stable against dissolution in the presence of ZAβ3, 15 µM preformed dimAβ:ZAβ3W complex was incubated over one week in the presence of 48 µM (in monomer equivalents) sonicated dimAβ RF seeds and the wavelength of maximum tryptophan fluorescence emission was recorded as previously described.[6]

Modeling of biphasic assembly kinetics

To replicate the experimentally observed transition from sigmoidal to biphasic growth we performed numerical simulations for fibril growth in the presence of off-pathway aggregation. To do so we modified the model of Powers and Powers (for details, see ref. 7) in three ways. We (i) accounted for secondary nucleation of fibril growth; (ii) replaced the off-pathway amorphous precipitates with off-pathway oligomers that could only form after crossing a well-defined solubility threshold we had previously identified;[2] and again following our experimental results, we (iii) assumed that RF fibrils, once nucleated, elongate faster than gO/CFs grow. A more detailed description of this model is provided further below.

To connect ThT responses to the kinetics of gO/CF vs. RF formation, we built on our prior measurements indicating that ThT responses to gO/CFs are weaker than to equivalent concentrations of RFs (about ten times in the case of hewL).[8] We further considered the ThT fluorescence to be the linear superposition of the response evoked by gO/CFs and RFs, each with their distinct response factors, i.e.

$$\Delta ThT = \alpha\,[gO, CF] + \beta\,[RF]$$

The fits used α, β as global fitting parameters for a given protein. This implicitly assumes that binding of ThT to gO/CFs and RFs remains linear over the range of concentrations we consider.

Assessing role of hewL hydrolysis

We have previously shown that hewL hydrolysis under our growth conditions requires in excess of 18 hours to generate distinct peptide fragments (see Fig. 4 in ref. 8). Since gO/RF formation is lag-free and the total amounts of gO/CFs formed at the plateau phase matched monomer concentrations above the COC (see ref. 2), hydrolysis is unlikely to underlie gO/CF formation in our system. In contrast, RF formation does show lag periods that stretch into the time frame for weak hewL hydrolysis. To investigate whether hydrolysis does affect RF formation under our growth conditions, we pre-hydrolyzed 20 mg/ml of hewL monomers in 25 mM KH_2PO_4 buffer (RF growth conditions) for either 3 or 7 days at 45 °C, ie. slightly below the threshold temperature of 50 °C for any amyloid aggregation.

NMR spectroscopy

For solution NMR spectroscopy, [U-^{15}N]-dimAβ was freshly eluted in 20 mM Na-phosphate, 50 mM NaCl, pH 10, from a Superdex 75 10/300 column (GE Healthcare). 375 µl eluate at ca. 130 µM protein concentration was diluted with 75 µl of 20 mM NaH_2PO_4, 50 mM NaCl, and 50 µl D_2O to a final [U-^{15}N]-dimAβ concentration of ca. 100 µM. The solution had a pH of 7.9. For comparison with dimAβ, [U-^{15}N]-Aβ40 was prepared with an N-terminal methionine as described previously.[1] Solution NMR data were collected at 5 °C using a 600 MHz spectrometer (Varian). [^{1}H,^{15}N]-HSQC spectra were collected at 5.0°C on a Bruker AVANCE III HD 600 MHz or Varian VNMRS 900 MHz NMR spectrometer equipped with cryogenic probes with z-axis pulsed field gradient capabilities.

For solid-state NMR spectroscopy, [U-^{15}N-^{13}C]-dimAβ was freshly eluted in 20 mM Na-phosphate, pH 10, from a Superdex 75 16/60 column (GE Healthcare). To form RFs samples were incubated in 5 ml Qualyvials (Zinsser). 1035 µl isotopically labeled dimAβ were mixed with 3915 µl 20 mM Na-phosphate, 50 mM NaCl, pH 7.4, and 50 µl 10% NaN_3. The vials were incubated at 37 °C while being stirred with a micro stir bar. After 20 h of incubation fibril formation was confirmed by AFM analysis. The remaining sample was centrifuged for 10 min at 16.100 x g at 4 °C, and the pellet was centrifuged into a 3.2 mm MAS NMR rotor. MAS NMR spectra were recorded at sample temperatures of 25 °C $\pm$ 5 °C (INEPT spectrum, Fig. S2B) and 0 °C $\pm$ 5 °C (PDSD spectrum with CP excitation, Fig. S2C), respectively on a 14.1 T (^{1}H Larmor frequency: 600 MHz) spectrometer (Varian). NMR data were processed with NMRPipe[9] using squared and shifted sine bell functions for apodization and analyzed with CcpNmr.[10]

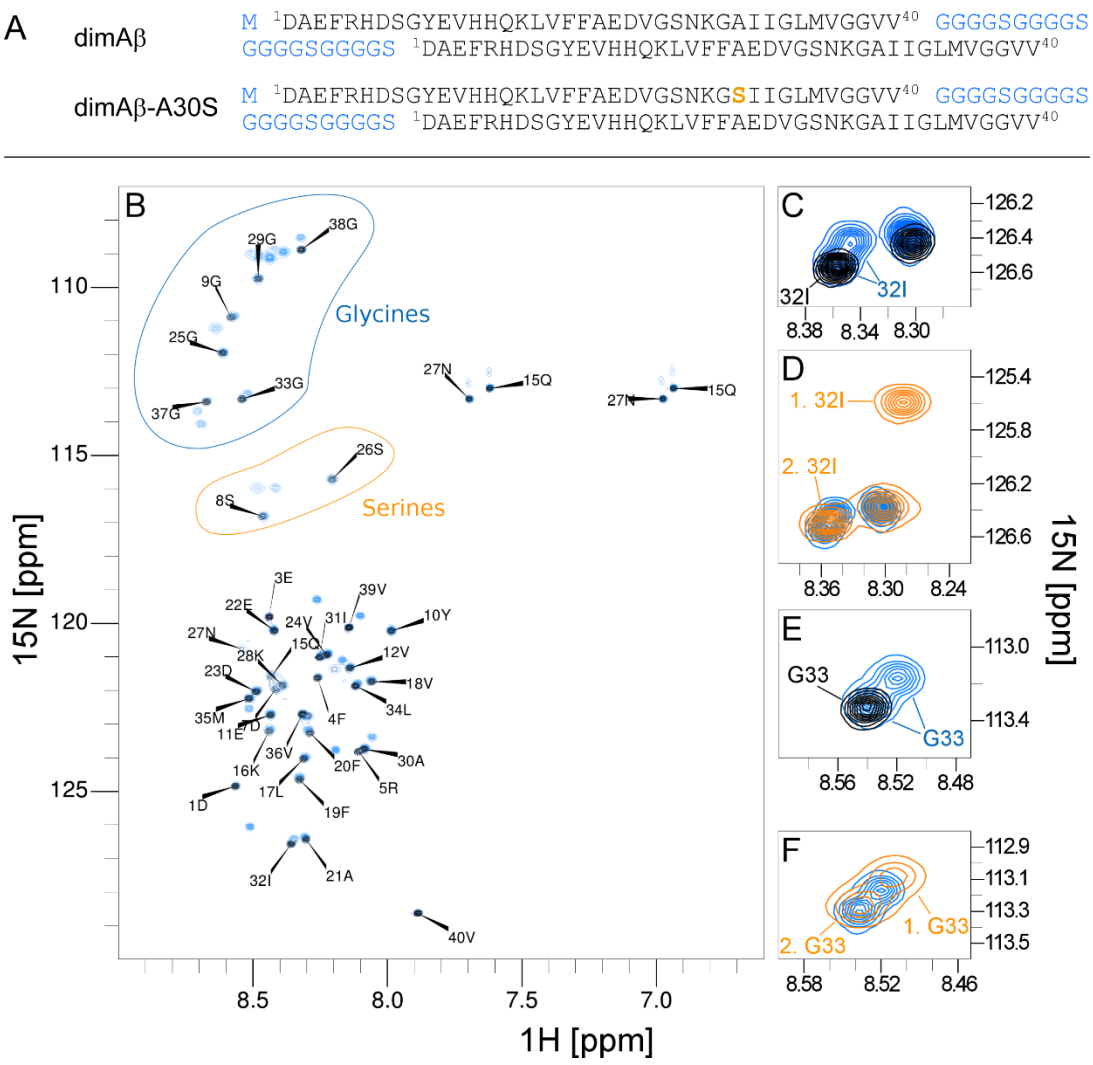

Figure S1. The conformation of monomeric Aβ40 is retained in dimAβ. To assess differences in conformation, solution NMR spectra of monomeric Aβ40 were compared to those of monomeric dimAβ and the mutant dimAβ-A30S. (**A**) Amino acid sequences of dimAβ and dimAβ-A30S. DimAβ-A30S contains an Ala-to-Ser exchange at position 30 of only the first Aβ40 unit, in order to locally perturb the NMR spectrum and abolish spectral overlap of the two Aβ40 units. (**B**) Overlay of (^{1}H-^{15}N) HSQC NMR spectra of [U-^{15}N]-Aβ40 (black) and [U-^{15}N]-dimAβ (blue). Assignments are shown for Aβ40. In the spectrum of [U-^{15}N]-dimAβ the resonances of Aβ40 are recovered, indicating that the conformation of monomeric Aβ40 is retained in dimAβ. In addition, further peaks are observed mainly in the glycine and serine regions of the spectrum and can be attributed to the $(G_4S)_4$ linker. For some resonances in the central/C-terminal region of the Aβ sequence, e.g., Ile-32 and Gly-33, peak splittings are evident in the spectrum of dimAβ (**C**,**E**). To evaluate if the peak splittings originate from a symmetric interaction between both Aβ units, or if it is due to the asymmetric placement of the Aβ units within dimAβ (preceding vs. following the linker), the variant dimAβ-A30S was generated and compared to dimAβ. In dimAβ-A30S (orange spectrum), one of the two split resonances observed for dimAβ is shifted as a consequence of local perturbation by the A30S mutation (**D**,**F**). This indicates that the peak splittings are not due to a symmetric interaction between both Aβ units, as in this case quadruple peaks would be expected for Ile-32 and Gly-33. Instead, specifically the one dimAβ resonance is shifted in dimAβ-A30S (D,F) that does not overlay with the Aβ40 resonance (C,E). This suggests that the peak splittings in dimAβ result from a slightly altered electronic environment of the central/C-terminal region in the N-terminal Aβ unit within dimAβ, likely resulting from proximity to, or transient interaction with, the linker region.

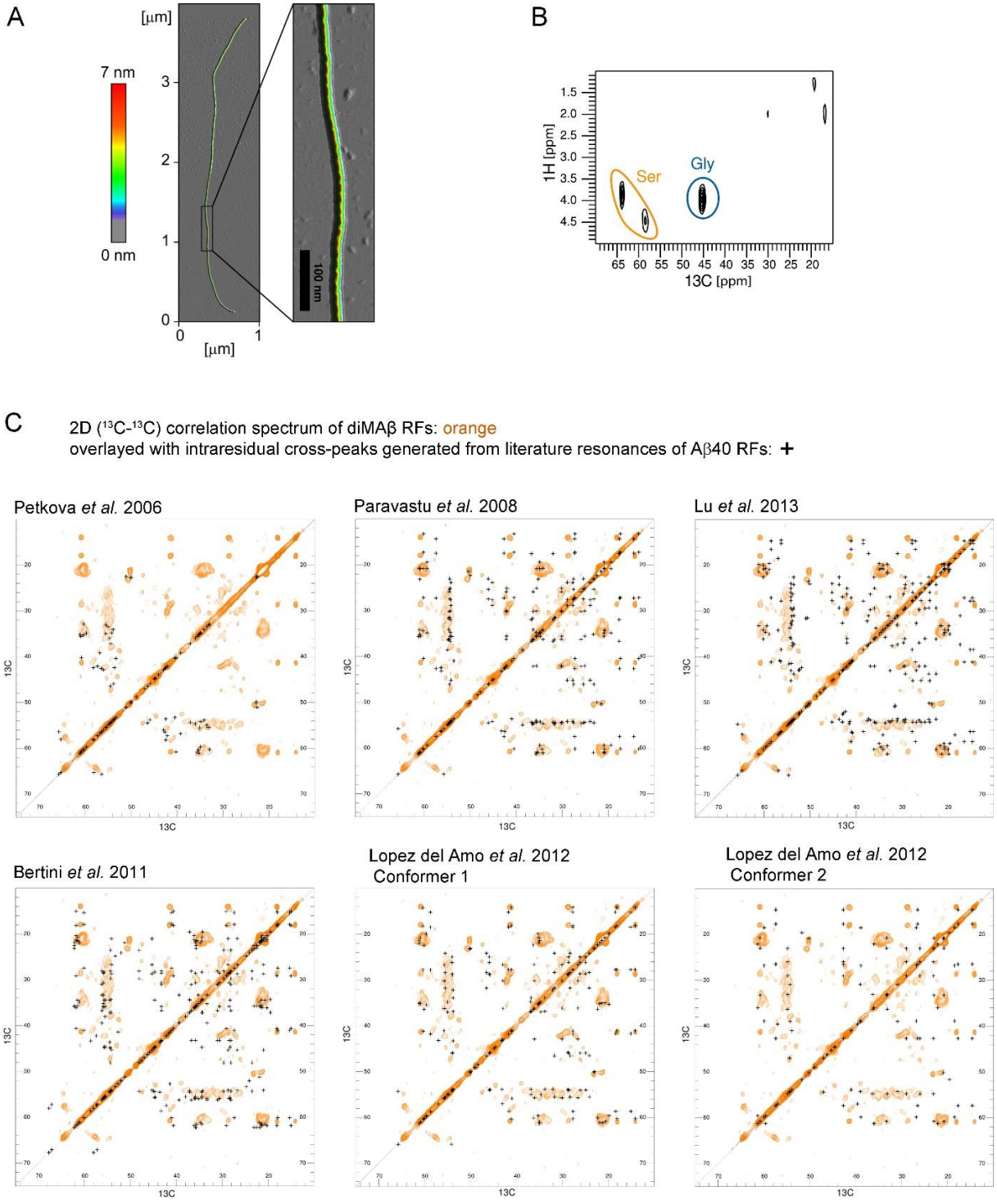

Figure S2. Both Aβ subunits of dimAβ are incorporated into the RF β-sheet core. (**A**) AFM image of a dimAβ RF. Color scale: height in nm. (**B**) 2D (^{1}H-^{13}C) HETCOR spectrum obtained with refocused INEPT as magnetization transfer[11] of diMAβ RFs. Only signals from mobile regions of the fibrils are detected.[12] Almost exclusively signals from glycine and serine residues (encircled) in dimAβ RFs are visible, indicating that the $(G_4S)_4$ linker remains flexible, while both Aβ units are incorporated into the RF β-sheet core. The sample temperature was ~25 °C ± 5°C, the MAS spinning speed was 11 kHz. For the 2D spectrum, 64 t_1 increments with 32 scans each were recorded. During ^{13}C detection, high-power proton decoupling (~83 kHz) was applied. (**C**) 2D (^{13}C-^{13}C) correlation spectrum of diMAβ RFs (orange) overlayed with intraresidual cross-peaks generated from resonances previously reported for six preparations of Aβ40 RFs (crosses). Initial proton to carbon magnetization transfer was achieved by cross polarization with a contact time of 200 µs,

homonuclear mixing was achieved by proton driven spin diffusion with a mixing time of 50 ms. High-power proton decoupling (~83 kHz) was employed during ^{13}C evolution and detection periods. Sample temperature was ~0 °C $\pm$ 5°C, the spinning speed was 11 kHz. In total 256 t_1 increments with 128 scans each were recorded. MAS NMR was performed at a magnetic field strength of 14.1 T corresponding to a proton Larmor frequency of 600 MHz. Spectra were processed using squared and shifted sine-bell apodization (shift of 0.35·π). The Aβ40 RF literature resonances are from Petkova *et al.* (BMRB entry 18127),[13] Paravastu *et al.* (BMRB entry 18129),[14] Lu *et al.* (BMRB entry 19009),[15] Bertini et al.,[16] and Lopez del Amo *et al*.[17] The spectrum of diMAβ RFs particularly overlaps with the cross-peaks of conformer 1 of Lopez del Amo *et al.*, but also with those of Bertini et al., Petkova *et al.*, and Paravastu *et al.*, suggesting structural similarity of the diMAβ RF polymorph investigated here with the Aβ40 RF polymorphs of these studies.

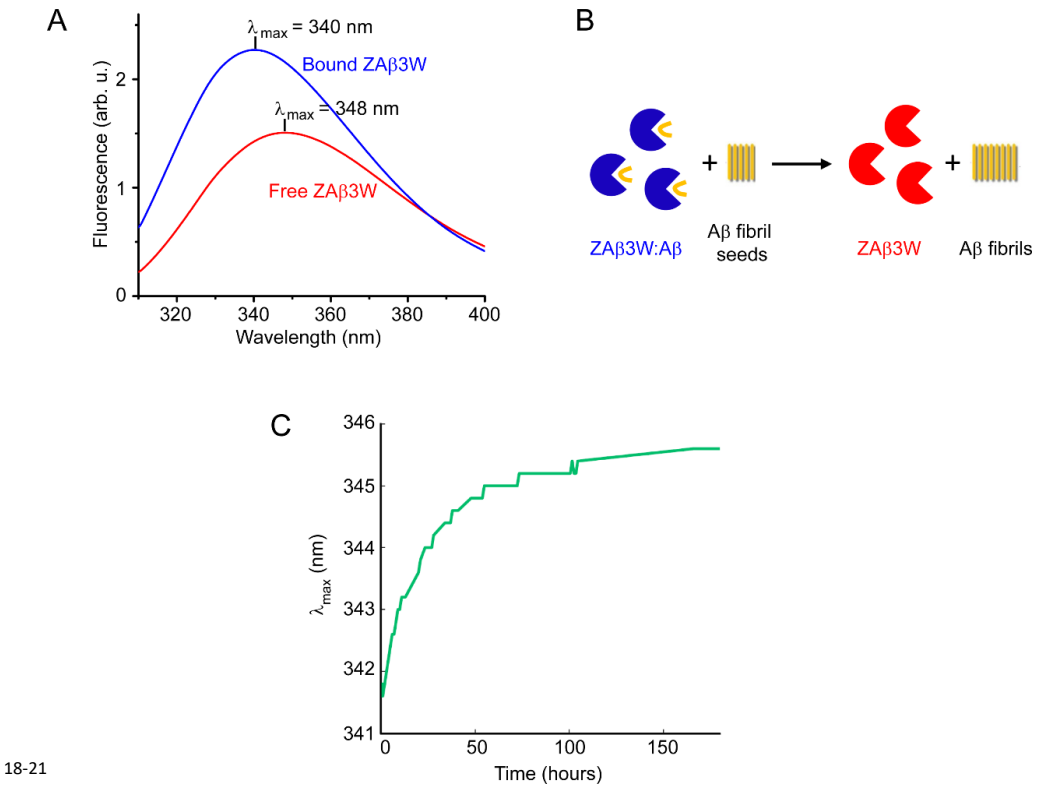

Figure S3. DimAβ possesses higher thermodynamic stability in the RF state than in the ZAβ$_3$-bound state. (**A**) ZAβ3W, a tryptophan-containing version of ZAβ3, is a probe for the stability of Aβ assembly states.[6] The fluorescence emission spectrum of ZAβ3W exhibits a blue shift upon binding of Aβ and can therefore report on dissociation of Aβ monomers from Aβ assemblies. (**B**) Scheme of the experiment to compare the thermodynamic stability of dimAβ in the ZAβ$_3$-bound and RF state. 15 µM preformed dimAβ:ZAβ3W complex was incubated over one week in the presence of 48 µM (in monomer equivalents) sonicated dimAβ RF seeds and the wavelength of maximum tryptophan fluorescence emission was recorded as described previously.[6] (**C**) The wavelength of maximum tryptophan fluorescence emission exhibits a red shift, indicating that dimAβ dissociates from the dimAβ:ZAβ3W complex and is incorporated into RFs.

Kinetic Model of Competing Oligomer and Fibril Pathways

Our formalism for the transition from sigmoidal to biphasic growth upon crossing the COC builds on the model of Powers and Powers.[22] Their original model has two assembly pathways: (1) on-pathway assembly leads to RF formation, and (2) off-pathway assembly generating gOs. We include both pathways in our model. Along the on-pathway, the fibril nucleation barrier is represented by unfavorable association constants for monomer addition up to n=5 (nucleus size). Note that the reaction rates can be adjusted to fit the model to the data when a nucleus size smaller or larger than 5 is considered. The reaction from nucleus to RF is irreversible (note that $b_2 = 0$). The unstructured oligomer growth is treated as unstable aggregates that may grow to some specified maximum size, m (we take m=8), and follow the off-pathway that essentially buffers the monomer concentration temporarily. This, for now, neglects subsequent assembly of gOs in CFs.

To replicate our observations, we make four key changes to the model by Powers and Powers. (1) We use rate constants that are significantly smaller than those in (Powers and Powers 2008).[22] (2) In the original model, the same on-rate for monomer addition was used along the entire on-pathway, while the off-rate below and above the nucleus size were different. In our model, both the on- and off rates (a_1 vs. a, and b_1 vs. b in Fig. S4) are different for aggregates that are smaller than the nucleus size and RFs. (3) We included a secondary nucleation mechanism, as proposed by Knowles et al.[3,4,23,24] where already formed RFs facilitate nucleation of new seeds (blue arrows, k_2 binding constant in Fig. S4). This was necessary to replicate the sharp autocatalytic rise in the experimental ThT fluorescence upon RFs nucleation. (4) To incorporate the lack of gO formation below the COC and the dependence of experimental gO growth rates on monomer concentration, we replicated the increase in off-pathway assembly rates seen in experiment (see Fig. 4C, insert). With these changes, the amount of different species in the solution are given by the following rate equations.

$$\frac{d[X_1]}{dt} = -[X_1](2a_1[X_1] + a_1\sum_{j=2}^{n}[Y_j] + a[F^{(0)}]) + 2b_1[Y_2] + b_1\sum_{j=3}^{n}[Y_j] + c[F^{(0)}] - [X_1](2\alpha_1[X_1] + \alpha\sum_{j=2}^{m}[Z_j]) + 2\beta[Z_2] + \beta\sum_{j=3}^{m}[Z_j] - k_2 n[X_1]^n[F^{(1)}] \quad (1)$$

$$\frac{d[Y_2]}{dt} = (a_1[X_1]^2 - b_1[Y_2]) - (a_1[X_1][Y_2] - b_1[Y_3]) \quad (2)$$

$$\frac{d[Y_j]}{dt} = (a_1[X_1][Y_{j-1}] - b_1[Y_j]) - (a_1[X_1][Y_j] - b_1[Y_{j+1}]),\ j=3,4. \quad (3)$$

$$\frac{d[Y_n]}{dt} = (a_1[X_1][Y_{n-1}] - b_1[Y_n]) - a[X_1][Y_n] + k_2[X_1]^n[F^{(1)}] \quad (4)$$

$$\frac{d[Z_2]}{dt} = (\alpha_1[X_1]^2 - \beta\ \ [Z_2]) - (\alpha[X_1][Z_2] - \beta[Z_3]) \quad (5)$$

$$\frac{d[Z_j]}{dt} = (\alpha[X_1][Z_{j-1}] - \beta[Z_j]) - (\alpha[X_1][Z_j] - \beta[Z_{j+1}]),\ j=3,4,\ldots 7. \quad (6)$$

$$\frac{d[Z_m]}{dt} = (\alpha_1[X_1][Z_{m-1}] - \beta[Z_m]) \quad (7)$$

$$\frac{d[F^{(0)}]}{dt} = a[X_1][Y_n] \quad (8)$$

$$\frac{d[F^{(1)}]}{dt} = (n+1)a[X_1][Y_n] + a[X_1]\left[F^{(0)}\right] - c[F^{(0)}], \quad (9)$$

where $[X_1]$, $[Y_j]$, $[Z_j]$, $[F^{(0)}]$, and $[F^{(1)}]$ represent the concentration of monomers, i-mers along the on-pathway, j-mers along the off-pathway, the RF number concentration, and the amount of monomers incorporated in RFs respectively in μM. The last term in eqs (1 – 5) each corresponds to secondary nucleation of new fibrils catalyzed by already established ones. The rate constants, a, b_1, c, and β are fixed at 1.98×10^{11} $M^{-1}hr^{-1}$, 3.96×10^{-4} hr^{-1}, 7.2×10^{2} hr^{-1}, and 3.6×10^{-2} hr^{-1} respectively. The on rate, α_1, is given by $7.2\times10^{10} \times f([X_1],[NaCl])$ (in $M^{-1}hr^{-1}$), where $f([X_1],NaCl)$ is given by the following equation

$$f([X1], NaCl) = \frac{1}{1 + exp^{(COC-[X_1])/0.5}}$$

$$COC = 3.522e^{-[NaCl]/45.3107} + 45.3107$$

where COC is the critical oligomer concentration. This assures that the oligomer reaction only becomes significant upon crossing the COC. In the model, the primary and secondary nucleation rates a_1 and k_2 are varied over the range 6.336 $M^{-1}hr^{-1}$ – 10.296 $M^{-1}hr^{-1}$ and 3.6×10^{-15} $M^{-1}hr^{-1}$ – 5.04×10^{-10} $M^{-1}hr^{-1}$ to obtain the best fit for fibril and aggregation growth with varying initial monomer concentration. The rate constant α is varied between 72.0 $M^{-1}hr^{-1}$ – 1.728×10^{3} $M^{-1}hr^{-1}$ to stay consistent with the power law behavior of the initial slope of gOs growth curve as a function of monomer concentration.

Representative time traces from the model with initial monomer concentration below and above the COC are shown in Figure S4B. In order to compare the theoretical mass concentrations to experimental ThT kinetics, we measured a slope of 125 ThT units / 1 μM RF for our plate reader. Based on our earlier measurements, the ThT response of gO/CFs was taken to be ten-fold weaker than that of RFs.[8]

A

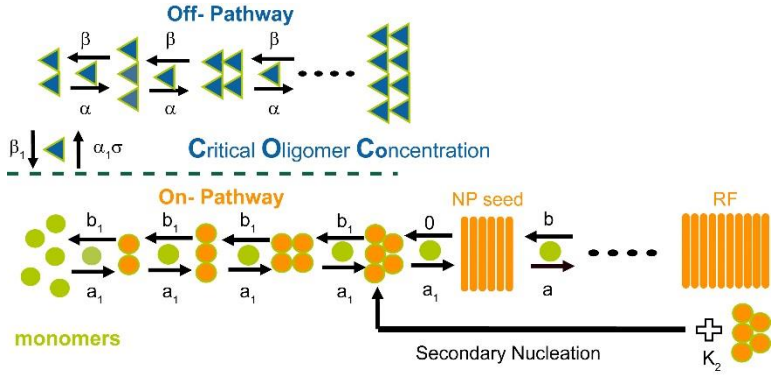

B

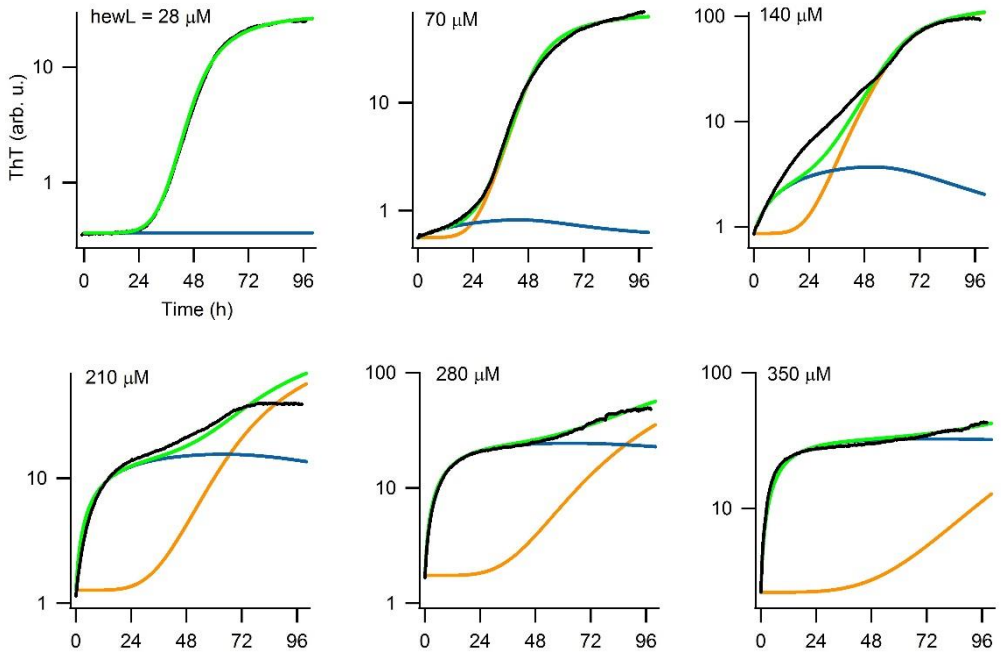

Figure S4: (**A**) Diagram of on- and off-pathways in the kinetic model. The on-pathway is displayed using orange symbols, where in addition to primary nucleation, secondary nucleation contributes to RF seed formation. Within the on-pathway, monomers (green) associate, forming pre-fibrillar multimers (orange) until eventually reaching a nucleus size (orange bars) consisting of n monomers. Beyond this specified nucleus, fibril growth begins. Already existing fibrils catalyze the formation of new ones through secondary nucleation with rate constant K_2. On the off-pathway monomers form gOs, but can only do so once monomer concentrations cross the COC. This limits the pool of monomers available for gO growth (indicated by using triangles instead of spheres) (**B**) Comparison of simulated with experimental kinetics. Experimental observed time-traces (black) showing ThT kinetics in response to the presence of hewl gOs and RFs and theoretical fits (green) plotted alongside their contributions from gOs (blue) and RFs (orange) concentrations at the indicated total monomer concentrations. ThT increases are in arbitrary units but account for the 10-fold smaller ThT response to equivalent mass concentrations from gO/CFs vs. RFs.

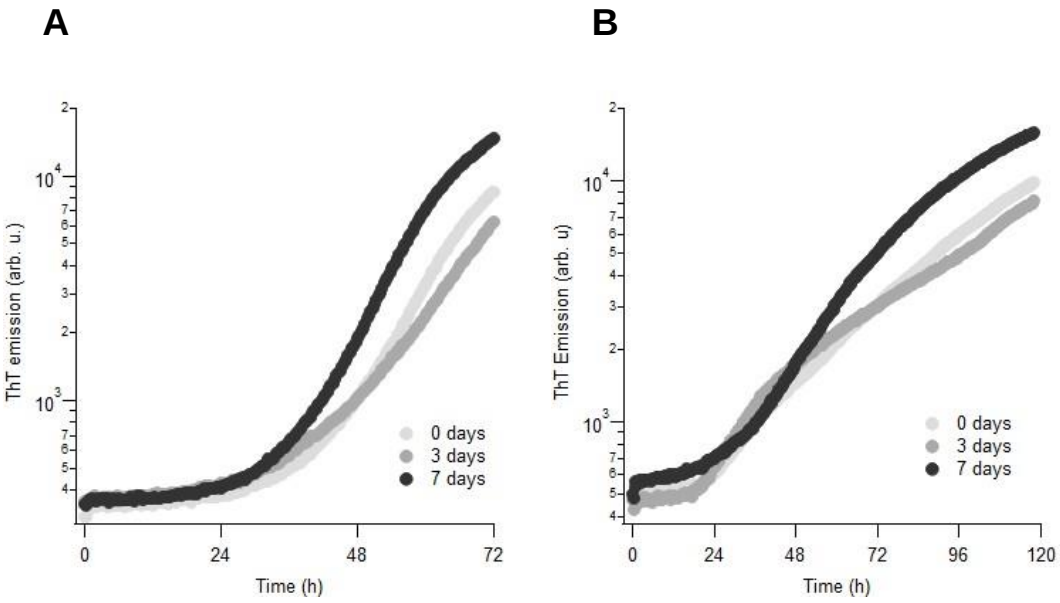

Figure S5: Effect of hewL pre-hydrolysis on RF nucleation and growth. HewL monomers, either freshly prepared or pre-hydrolyzed for 3 or 7 days, were incubated at (A) 30 uM hewL and 350 mM NaCl or (B) 350 uM and 100 mM NaCl in the presence of 15 uM ThT. Both are RF growth conditions, but at more than 10-fold different protein concentrations. As shown, pre-hydrolysis did not affect the RF lag periods in our system. Some acceleration in RF elongation occurred during the latter parts of the incubation periods, and only for the 7 day pre-hydrolyzed sample. This suggests that hewL hydrolysis, under our growth conditions, is not the cause of RF nucleation but can accelerate RF elongation rates at the late-stages of growth.

References

1. B. Macao, W. Hoyer, A. Sandberg, A.-C. Brorsson, C. M. Dobson and T. Härd, *BMC Biotechnol.*, 2008, **8**, 82.
2. T. Miti, M. Mulaj, J. D. Schmit and M. Muschol, *Biomacromolecules*, 2015, **16**, 326-335.
3. T. P. J. Knowles, C. A. Waudby, G. L. Devlin, S. I. A. Cohen, A. Aguzzi, M. Vendruscolo, E. M. Terentjev, M. E. Welland and C. M. Dobson, *Science*, 2009, **326**, 1533-1537.
4. S. I. A. Cohen, M. Vendruscolo, M. E. Welland, C. M. Dobson, E. M. Terentjev and T. P. J. Knowles, *J. Chem. Phys.*, 2011, **135**, 065105.
5. E. A. Mirecka, H. Shaykhalishahi, A. Gauhar, Ş. Akgül, J. Lecher, D. Willbold, M. Stoldt and W. Hoyer, *Angew. Chem. Int. Ed.*, 2014, **53**, 4227-4230.
6. C. S. R. Grüning, S. Klinker, M. Wolff, M. Schneider, K. Toksöz, A. N. Klein, L. Nagel-Steger, D. Willbold and W. Hoyer, *J. Biol. Chem.*, 2013, **288**, 37104-37111.
7. E. T. Powers and D. L. Powers, *Biophys. J.*, 2008, **94**, 379-391.
8. J. Foley, S. E. Hill, T. Miti, M. Mulaj, M. Ciesla, R. Robeel, C. Persichilli, R. Raynes, S. Westerheide and M. Muschol, *J. Chem. Phys.*, 2013, **139**, 121901/121901-121912.
9. F. Delaglio, S. Grzesiek, G. W. Vuister, G. Zhu, J. Pfeifer and A. Bax, *J. Biomol. NMR*, 1995, **6**, 277-293.
10. W. F. Vranken, W. Boucher, T. J. Stevens, R. H. Fogh, A. Pajon, M. Llinas, E. L. Ulrich, J. L. Markley, J. Ionides and E. D. Laue, *Proteins*, 2005, **59**.
11. R. Freeman and G. A. Morris, *J. Am. Chem. Soc.*, 1979, **101**, 760-762.
12. H. Heise, W. Hoyer, S. Becker, O. C. Andronesi, D. Riedel and M. Baldus, *Proc. Natl. Acad. Sci. USA*, 2005, **102**, 15871-15876.
13. A. T. Petkova, W. M. Yau and R. Tycko, *Biochemistry*, 2006, **45**, 498-512.
14. A. K. Paravastu, R. D. Leapman, W. M. Yau and R. Tycko, *Proc. Natl. Acad. Sci. USA*, 2008, **105**, 18349-18354.
15. J. X. Lu, W. Qiang, W. M. Yau, C. D. Schwieters, S. C. Meredith and R. Tycko, *Cell*, 2013, **154**, 1257-1268.
16. I. Bertini, L. Gonnelli, C. Luchinat, J. Mao and A. Nesi, *J. Am. Chem. Soc.*, 2011, **133**, 16013-16022.
17. J. M. Lopez del Amo, M. Schmidt, U. Fink, M. Dasari, M. Fandrich and B. Reif, *Angew. Chem. Int. Ed. Engl.*, 2012, **51**, 6136-6139.
18. Z. Fu, D. Aucoin, J. Davis, W. E. Van Nostrand and S. O. Smith, *Biochemistry*, 2015, **54**, 4197-4207.
19. A. Lomakin, D. S. Chung, G. B. Benedek, D. A. Kirschner and D. B. Teplow, *Proc. Natl. Acad. Sci. USA*, 1996, **93**, 1125-1129.
20. L. M. Luheshi, W. Hoyer, T. P. de Barros, I. van Dijk Härd, A.-C. Brorsson, B. Macao, C. Persson, D. C. Crowther, D. A. Lomas, S. Ståhl, C. M. Dobson and T. Härd, *PLoS Biol.*, 2010, **8**, e1000334.
21. M. Nick, Y. Wu, N. W. Schmidt, S. B. Prusiner, J. Stöhr and W. F. DeGrado, *Biopolymers*, 2018, e23096.
22. E. T. Powers and D. L. Powers, *Biophys J*, 2008, **94**, 379-391.
23. S. I. A. Cohen, M. Vendruscolo, C. M. Dobson and T. P. J. Knowles, *J. Chem. Phys.*, 2011, **135**, 065106/065101-065118.
24. S. I. A. Cohen, S. Linse, L. M. Luheshi, E. Hellstrand, D. A. White, L. Rajah, D. E. Otzen, M. Vendruscolo, C. M. Dobson and T. P. J. Knowles, *Proceedings of the National Academy of Sciences*, 2013, **110**, 9758-9763.